High-power, widely-tunable Cr^{2+}:ZnSe master oscillator power amplifier systems

P. A. Berry* and K. L. Schepler

Air Force Research Laboratory, Wright Patterson Air Force Base, OH 45433, USA
**patrick.berry@wpafb.af.mil*

Abstract: We demonstrate high-power Cr^{2+}:ZnSe master oscillator power amplifier (MOPA) pure continuous wave (CW) laser systems with output power of 14 W and amplifier gain greater than 2X. In addition, we develop a theoretical model for this type of amplification and show single-knob tunability at high powers over 400 nm.

OCIS codes: (140.3580) Lasers, solid-state; (140.3070) Infrared and far-infrared lasers.

References and links

1. L. D. DeLoach, R. H. Page, G. D. Wilke, S. A. Payne, and W. F. Krupke, "Transition metal-doped zinc chalcogenides: spectroscopy and laser demonstration of a new class of gain media," IEEE J. Quantum Electron. **32**(6), 885–895 (1996).
2. R. H. Page, K. I. Schaffers, L. D. DeLoach, G. D. Wilke, F. D. Patel, J. B. Tassano, Jr., S. A. Payne, W. F. Krupke, K. T. Chen, and A. Burger, "Cr^{2+}-doped zinc chalcogenides as efficient, widely tunable mid-infrared lasers," IEEE J. Quantum Electron. **33**(4), 609–619 (1997).
3. I. T. Sorokina, E. Sorokin, S. Mirov, V. Fedorov, V. Badikov, V. Panyutin, and K. I. Schaffers, "Broadly tunable compact continuous-wave Cr^{2+}:ZnS laser," Opt. Lett. **27**(12), 1040–1042 (2002).
4. U. Hömmerich, X. Wu, V. R. Davis, S. B. Trivedi, K. Grasza, R. J. Chen, and S. Kutcher, "Demonstration of room-temperature laser action at 2.5 mum from Cr^{2+}:$Cd_{0.85}Mn_{0.15}Te$," Opt. Lett. **22**(15), 1180–1182 (1997).
5. J. McKay, K. L. Schepler, and G. C. Catella, "Efficient grating-tuned mid-infrared Cr^{2+}:CdSe laser," Opt. Lett. **24**(22), 1575–1577 (1999).
6. U. Demirbas, and A. Sennaroglu, "Intracavity-pumped Cr^{2+}:ZnSe laser with ultrabroad tuning range between 1880 and 3100 nm," Opt. Lett. **31**(15), 2293–2295 (2006).
7. I. T. Sorokina, "Cr^{2+}-doped II-VI materials for lasers and nonlinear optics," Opt. Mater. **26**(4), 395–412 (2004).
8. I. S. Moskalev, V. V. Fedorov, S. B. Mirov, P. A. Berry, and K. L. Schepler, "12-Watt CW Polycrystalline Cr^{2+}:ZnSe Laser Pumped by Tm-fiber Laser," in *Advanced Solid State Photonics*(Optical Society of America, Denver, CO, 2008), p. WB30.
9. T. J. Carrig, G. J. Wagner, W. J. Alford, and A. Zakel, "Chromium-doped chalcogenide lasers," in *Solid State Lasers and Amplifiers*, A. Sennaroglu, J. G. Fujimoto, and C. R. Pollock, eds. (SPIE, Bellingham, WA, 2004), pp. 74–82.
10. G. J. Wagner, B. G. Tiemann, W. J. Alford, and T. J. Carrig, "Single-Frequency Cr:ZnSe Laser," in *Advanced Solid-State Photonics*(Optical Society of America, 2004), p. WB12.
11. E. Sorokin, I. T. Sorokina, M. S. Mirov, V. V. Fedorov, I. S. Moskalev, and S. B. Mirov, "Ultrabroad Continuous-Wave Tuning of Ceramic Cr:ZnSe and Cr:ZnS Lasers," in *Advanced Solid-State Photonics*(Optical Society of America, 2010), p. AMC2.
12. I. S. Moskalev, V. V. Fedorov, and S. B. Mirov, "10-watt, pure continuous-wave, polycrystalline Cr^{2+}:ZnS laser," Opt. Express **17**(4), 2048–2056 (2009).
13. R. J. Harris, G. T. Johnston, G. A. Kepple, P. C. Krok, and H. Mukai, "Infrared thermooptic coefficient measurement of polycrystalline ZnSe, ZnS, CdTe, CaF_2, and BaF_2, single crystal KCI, and TI-20 glass," Appl. Opt. **16**(2), 436–438 (1977).
14. D. M. Simanovskii, H. A. Schwettman, H. Lee, and A. J. Welch, "Midinfrared Optical Breakdown in Transparent Dielectrics," Phys. Rev. Lett. **91**(10), 107601 (2003).
15. K. L. Schepler, R. D. Peterson, P. A. Berry, and J. B. McKay, "Thermal Effects in Cr^{2+}:ZnSe Thin Disk Lasers," IEEE J. Sel. Top. Quantum Electron. **11**(3), 713–720 (2005).
16. P. A. Berry, and K. L. Schepler, "Cr^{2+}:ZnSe master oscillator / power amplifier for improved power scaling," in *Solid State Lasers XIX: Technology and Devices*(SPIE, San Francisco, California, USA, 2010), pp. 75781L–75711.
17. A. Sennaroglu, U. Demirbas, A. Kurt, and M. Somer, "Concentration dependence of fluorescence and lasing efficiency in Cr^{2+}:ZnSe lasers," Opt. Mater. **29**(6), 703–708 (2007).
18. H. Kogelnik, E. Ippen, A. Dienes, and C. Shank, "Astigmatically compensated cavities for CW dye lasers," IEEE J. Quantum Electron. **8**(3), 373–379 (1972).

#126243 - $15.00 USD Received 30 Mar 2010; revised 14 Jun 2010; accepted 23 Jun 2010; published 30 Jun 2010

1. Introduction

The atmospheric transmission windows in the middle-infrared (mid-IR, 2-5 μm) wavelength range, coupled with organic and other chemical absorption lines occurring throughout this region give rise to a wide variety of medical, scientific, commercial and military applications. Communications, remote sensing, IR countermeasures, laser surgery and non-invasive imaging are just a few of the drivers of high-power solid-state mid-IR laser development. Transition-metal doped II-VI laser materials, such as Cr^{2+}:ZnSe [1, 2], Cr^{2+}:ZnS [1–3], Cr^{2+}:$Cd_{1-x}Mn_xTe$ [4], and Cr^{2+}:CdSe [5], have many desirable properties such as wide tunability [6], broad absorption bands, a large gain cross section, room-temperature operation and no excited state absorption [1, 7].

Cr^{2+}:ZnSe in particular has been shown to be capable of continuous wave (CW) output power levels exceeding 12 W [8], gain switched lasing with average output power of up to 18.5 W [9], narrow-linewidth operation [10], and tunability from 1973 to 3339 nm [11]. Only relatively recently have higher-quality Cr^{2+}:ZnS crystals been fabricated and because of this, these types of lasers have not been as extensively demonstrated. However, they have been shown to be capable of multi-watt output [12], and can have some advantages over Cr^{2+}:ZnSe with respect to physical properties [13, 14]. Power scaling of chromium lasers has long been hampered by the problem of thermal lensing due to the high thermo-optic coefficients of zinc sulfide (46 x 10^{-6} 1/K), zinc selenide (70 x 10^{-6} 1/K), CdSe and CdTe (both ~100 x 10^{-6} 1/K) [7]. Self-focusing in the gain material leads to optical damage or cavity instability which limits the maximum achievable output power. These thermal issues can be addressed through appropriate choices of crystal geometry, a longer wavelength pump source and heat removal, all of which help to reduce the thermal load in the gain element [15]. Even when these steps are taken to mitigate the thermal problems, the lasers are often still limited in their output characteristics. One solution to this problem is to use a master oscillator power amplifier (MOPA) architecture where the MO design is chosen to emphasize a desirable operating characteristic such as beam quality, linewidth or tunability while the amplifier section accomplishes the power scaling without degrading performance.

In this paper we present MOPA laser performance using polycrystalline Cr^{2+}:ZnSe gain media in the conventional slab geometry for both the oscillator and the amplifier. We develop an improved amplifier gain model which incorporates variations in pump and signal beam parameters. We investigate a variety of MO configurations and their performance as part of a versatile MOPA-configuration laser system. We demonstrate 14 W of pure CW output and compare the system performance to the theoretical model. System versatility is demonstrated by multi-watt, narrow linewidth output tunable over a range greater than 400 nm. Beam quality and spectral content are also investigated.

2. Amplifier model

In order to design a MOPA Cr^{2+}:ZnSe laser, a theoretical model was developed and used to determine possible amplifier performance for a given set of physical parameters. We considered optical pumping co-aligned with an input signal beam. Absorption by the Cr^{2+} ions is proportional to pump intensity so both pump intensity and absorbed power will decrease along the propagation direction. In addition, both the pump and signal are expected to have some non-uniform transverse distribution which we will model as well.

Any amplifier model must be based on known or measured material parameters involved in absorption and emission. The absorption and emission cross-sections for Cr^{2+}:ZnSe vary in the literature (for example, between 0.9 x 10^{-18} and 1.3 x 10^{-18} cm^2 for peak emission cross-section). This model will use values published by DeLoach et. al. [1] but also acceptable would be those from Sorokina et. al. [7]. The absorption and emission cross-sections at the pump wavelength of 1.9 μm, σ_{pa} and σ_{pe} respectively, are 0.6 x 10^{-18} cm^2 and 0.3 x 10^{-18} cm^2 while the emission cross-section at the input signal wavelength of 2.5 μm, σ_{se}, is 0.9 x 10^{-18} cm^2. The Cr^{2+} doping level, n_o, is calculated from the measured amount of a small signal (i.e. not close to saturating or bleaching the absorption) beam power transmitted through a

#126243 - $15.00 USD Received 30 Mar 2010; revised 14 Jun 2010; accepted 23 Jun 2010; published 30 Jun 2010

Cr^{2+}:ZnSe sample. A typical value of n_0 is 1 x 10^{19} cm^{-3}(~0.04% atomic) The Cr^{2+} ion in a tetrahedral crystal field is a 4-level system with fast relaxation in the vibronic sublevels which means that n_o is effectively the sum of n^* and n_g, where n^* is the upper state population and n_g is the unexcited (ground state) population.

In the case of a collinearly-pumped amplifier (where both the pump and signal beams propagate in the z-direction), the intensity-driven n^* is not uniform with respect to z, but will decrease due to absorption of the pump. Thus the gain at each z location will also vary due to the intensity dependence of the pumping rate. In order to calculate gain, G, in our amplifier we need to understand the relationships between n^*, the pump intensity, I_p and the input signal intensity, I_s through a system of differential equations.

The differential equation for n^* will have a positive term from absorption at the pump wavelength and negative terms from spontaneous emission and stimulated emission at the signal wavelength. In addition to these, because the absorption and emission bands of Cr^{2+}:ZnSe overlap in the 1.9 μm region, there will also be a stimulated re-emission term at the pump wavelength as well. The absorption cross section at 2.5 μm is negligible in Cr^{2+}:ZnSe so there will be no absorption term at the signal wavelength. The differential equation for the pump radiation intensity will have negative terms from absorption and passive losses at the pump wavelength in addition to a positive term due to stimulated re-emission at the pump wavelength. The differential equation for input signal intensity has a gain contribution from stimulated emission and passive losses at the signal wavelength.

This system, an improvement on our previous work [16], can be described using (1-3),

$$\frac{\partial n^*(t,z,r)}{\partial t} = \frac{I_p(t,z,r)}{h\nu_p}\left(\sigma_{pa} n_g(t,z,r) - \sigma_{pe} n^*(t,z,r)\right) - \frac{I_s(t,z,r)\sigma_{se}}{h\nu_s} n^*(t,z,r) - \frac{n^*(t,z,r)}{\tau} \tag{1}$$

$$\frac{\partial I_p(z,r)}{\partial z} = I_p(z,r)\left[-\sigma_{pa}\left(n_0 - n^*(z,r)\right) + \sigma_{pe} n^*(z,r) - \gamma_p\right] \tag{2}$$

$$\frac{\partial I_s(z,r)}{\partial z} = I_s(z,r)\left(\sigma_{se} n^*(z,r) - \gamma_s\right) \tag{3}$$

where υ_p and υ_s are the pump and signal frequencies, γ_p and γ_s are the passive losses at the pump and signal wavelengths, and τ is the lifetime of the excited state. At equilibrium and with no other time-dependence, we can solve (1) to get (4).

$$n^*(z,r) = \frac{\frac{I_p(z,r)}{h\nu_p}\sigma_{pa} n_0}{\frac{I_p(z,r)}{h\nu_p}\left(\sigma_{pa} + \sigma_{pe}\right) + \frac{I_s(z,r)}{h\nu_s}\sigma_{se} + \frac{1}{\tau}} \tag{4}$$

For a Cr^{2+} doping level of n_0, at room temperature τ is typically about ~4 μs [17]. It is interesting to note that the limit of (4) as intensity increases, for a pump wavelength of 1.9 μm, is as in (5),

$$\lim_{I_p \to \infty}\left(n^*\right) = \frac{\sigma_{pa}}{\sigma_{pa} + \sigma_{pe}} n_0 \tag{5}$$

which in this case means that n^* can reach a maximum of $2/3n_0$.

It is convenient to define the pump and signal intensities in dimensionless units so that we have (6) and (7),

#126243 - $15.00 USD Received 30 Mar 2010; revised 14 Jun 2010; accepted 23 Jun 2010; published 30 Jun 2010

$$J_p(z,r) = \frac{I_p(z,r)}{h\nu_p}\left(\sigma_{pa} + \sigma_{pe}\right)\tau = \frac{I_p(z,r)}{I_{p,sat}} \tag{6}$$

$$J_s(z,r) = \frac{I_s(z,r)}{h\nu_s}\sigma_{se}\tau = \frac{I_s(z,r)}{I_{s,sat}} \tag{7}$$

where $I_{s,sat}$ and $I_{s,sat}$ are the saturation intensities for signal and pump wavelengths. With these definitions, neglecting radial dependence and assuming negligible passive losses gives the system in (8-10).

$$n^*(z) = n_0 \frac{\sigma_{pa}}{\left(\sigma_{pa} + \sigma_{pe}\right)} \frac{J_p(z)}{J_p(z) + J_s(z) + 1} \tag{8}$$

$$\frac{dJ_p(z)}{dz} = J_p(z)\left[-\sigma_{pa} n_0 + \left(\sigma_{pa} + \sigma_{pe}\right) n^*(z)\right] \tag{9}$$

$$\frac{dJ_s(z)}{dz} = J_s(z)\sigma_{se} n^*(z) \tag{10}$$

These equations can be solved numerically for some initial pump and signal intensities, I_{p0} and I_{s0} and a crystal length L. This system assumes that both the signal and pump beams of a given power have a uniform transverse intensity over a circular area A (with say a radius of r). In practice, however, the pump and signal beams both have some non-uniform, mostly Gaussian transverse intensity distribution. In order to model the radial dependence, we must run the z-propagation model for points along the radius with intensities given by the Gaussian distribution (11) of r (with a $1/e^2$ radius of δ and a Gaussian order N) and integrate them over r and θ to get an output power.

$$I(r,\delta,N) = \exp\left(-\frac{2r^{2N}}{\delta^{2N}}\right) \tag{11}$$

This can take into account non-uniform saturation effects in the center of the signal beam where intensities are higher. The end result of which could be beams which become less Gaussian as they are amplified.

A working model was developed in MATLAB to represent our desired experimental configuration. Example model predictions of amplifier performance as a function of varying input signal levels and spot sizes can be seen in Fig. 1 below for a crystal length of 7.8 mm. The pump depletion level is shown by the comparison of the pump line with signal and without. At lower pump levels, this difference is not significant, but at higher powers the difference is appreciable, arguing for shorter amplifier lengths than a standard Beer's law model would specify for optimal absorption. The gain shows little sign of saturation effects due to pump or signal intensities until very high values (~10^{10} W/m^2). The information gained from the model results was used in the next section to drive the experimental design of the MOPA system. From these models, the amplifier efficiency for a typical beam size of 40-80 μm radius is around 50%, which is similar to the types of efficiencies we see in high power laser oscillators. Therefore, as long as good extraction efficiency can be achieved experimentally, this approach is very promising for power scaling of Cr^{2+}:ZnSe laser systems.

#126243 - $15.00 USD Received 30 Mar 2010; revised 14 Jun 2010; accepted 23 Jun 2010; published 30 Jun 2010

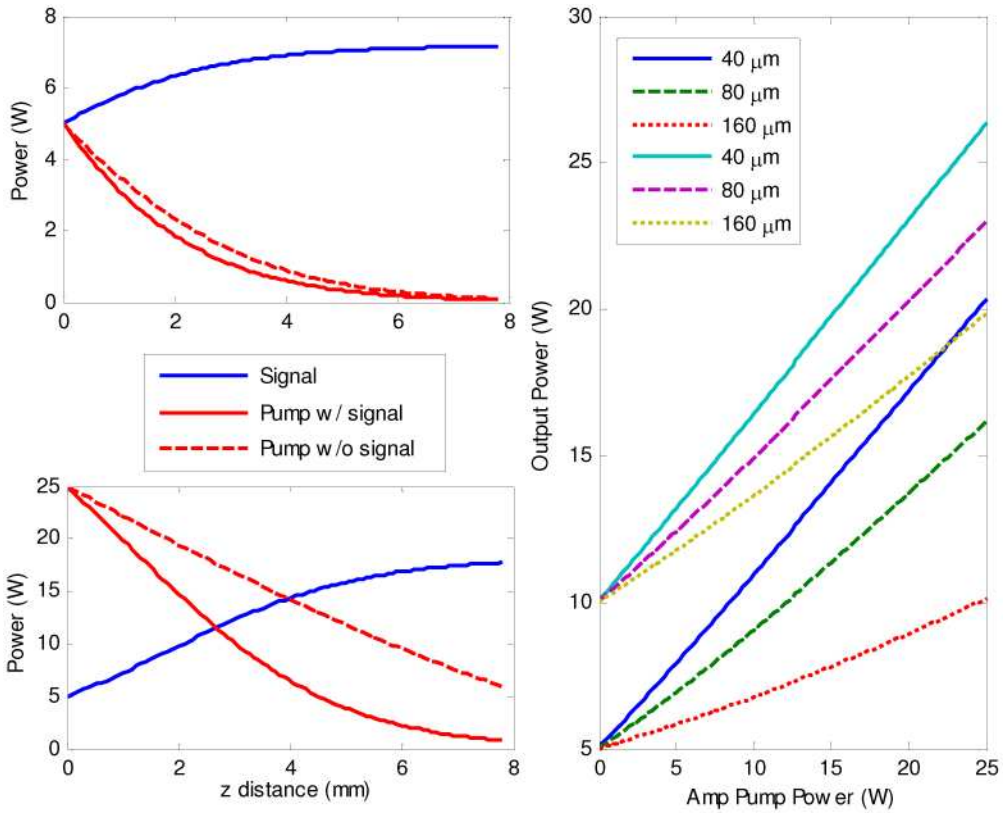

Fig. 1. Example model predictions showing (left) input signal growth and pump absorption (with signal present and without), over the crystal length for 5 W input signal and (top) 5 W pump and (bottom) 25 W pump, all at 80 μm spot size. Also shown (right) are amplification comparisons for 5 and 10 W input signal powers with varying spot size as a function of pump power.

3. Experimental design

One of the advantages of the MOPA design is the flexibility to use almost any combination of oscillator and amplifier. A variety of MO designs were built and tested with the simplest PA design. This was done to evaluate the advantages of each design while adhering to the optimum PA design with respect to simplicity and performance predicted by the model. MO designs were selected for their ability to optimize certain operating modes such as tunability, narrow linewidth or power output.

There are a number of situations which may require the orientation of the laser crystal at Brewster's angle in a laser cavity. Anti-reflective (AR) coatings in the 2-3 μm region may be too costly or not robust enough for use and thus another method is needed to reduce reflective losses. However, using a crystal at Brewster's angle carries with it some negative astigmatism effects which are compounded by thermal lensing in the crystal which is now at an angle. To counteract this, advantage can be taken of the astigmatism-compensating properties of cavity configurations first used by Kogelnik in dye laser cavities [18].

#126243 - $15.00 USD Received 30 Mar 2010; revised 14 Jun 2010; accepted 23 Jun 2010; published 30 Jun 2010

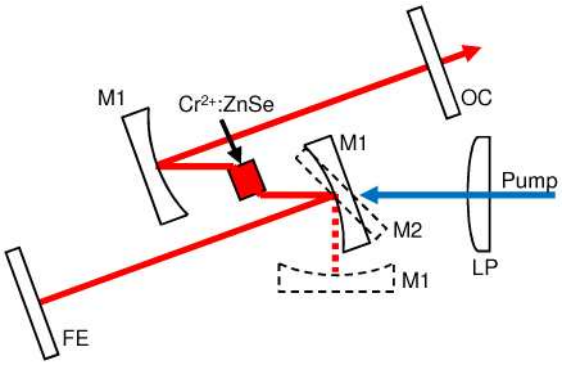

Fig. 2. Astigmatically-compensated *Z*-cavity design which can use either a single collimated-leg design (dashed) or a double-collimated leg design. OC = output coupler, LP = laser pump lens, FE = functional element.

Our initial approach used a Kogelnik-type cavity with a single collimated leg represented in Fig. 2 by the dashed lines. The cavity consisted of a flat 45° dichroic input coupler (M2), AR-coated for 1.9 µm and high reflectivity (HR)-coated for 2-3 µm; two 5 cm radius of curvature (ROC) spherical mirrors (M1); and a flat CaF_2 50% reflective (R) output coupler (OC) located ~16 cm from M1. The pump focusing lens (LP) had an experimentally-determined optimal focal length of 5 cm. The polycrystalline, 8.9x7.0x3.0 mm (LxWxH) Cr^{2+}:ZnSe gain element was pumped along the long dimension with a Tm-fiber laser linearly polarized parallel to the plane of the diagram. The fiber nature of the pump system and the lack of high-power isolators at 1.9 µm required that this and all subsequent designs incorporate a non-normal incidence input coupler to prevent back-reflection. This cavity was shown to be capable of over 12 W of pure CW power [8]. This single-leg cavity was limited however, in that its output beam quality and stability were poor at higher operating powers which essentially precluded quality focusing and overlap in the amplifier. It also had no good location in which to insert functional elements such as a grating for tunability or a saturable absorber for modelocking.

To address these concerns, a double collimated-leg *Z*-cavity was assembled as illustrated with the solid elements in Fig. 2. The same 5 cm ROC mirror (M1) used as an end mirror in the above cavity was moved one focal length from the gain element and used as the input coupler while also creating the second collimated leg. The ~16 cm long 'functional element' (FE) leg was terminated with a planar HR mirror for free-running mode or a 300 gr/mm, 2.5 µm blazed grating in the Littrow configuration for tuning and line narrowing. It was found experimentally that the optimal pump lens (LP) focal length was 7.5 cm and optimal outcoupler reflectivity was 70%. Modeling cavity mode overlap with the pump can be accomplished using a standard ABCD matrix method, but the results were merely a good starting point experimentally due to the variable and strong nature of the thermal lensing.

When robust AR coatings are available, some of the astigmatism problems can be eliminated by utilizing a normal-incidence *L*-cavity pumping scheme. This simplifies the cavity considerably as seen in Fig. 3A. Cavity stability can be achieved using either a concave HR end mirror (L_a-cavity) or a planar HR end mirror with an intracavity AR coated positive lens (L_b-cavity). The latter configuration is more complicated to construct in confined quarters and may have some loss depending on the quality of the AR coating but M2 could be replaced with a grating in the Littrow configuration to achieve cavity tuning. Both cavities had an optimal outcoupler reflectivity of 70% and pump lens focal lengths of 5 cm.

#126243 - $15.00 USD Received 30 Mar 2010; revised 14 Jun 2010; accepted 23 Jun 2010; published 30 Jun 2010

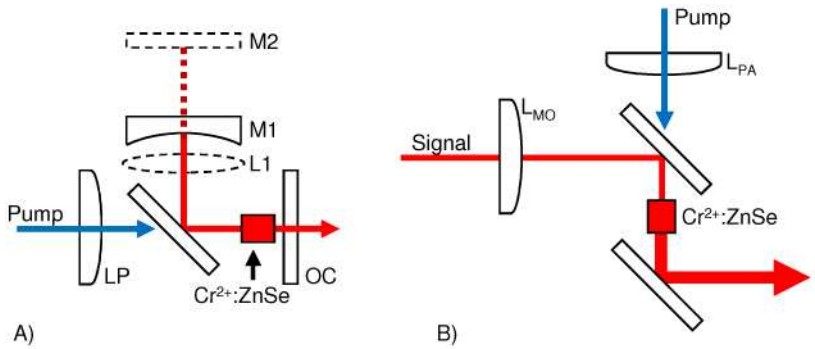

Fig. 3. A) Normal-incidence *L*-cavity scheme which can use either an HR curved mirror (M1) or a combination of planar HR (M2) and positive lens (L1). B) Power amplifier design where L_{MO} and L_{PA} are chosen for optimal overlap of pump and signal beams.

The power amplifier section used a co-linearly pumped, polycrystalline, 8.9x7.0x3.0 mm (LxWxH) Cr^{2+}:ZnSe crystal similar to the MO crystal, but AR coated for 1.9-3 µm. As seen in Fig. 3B, the 150 W maximum, 1.9 µm, Tm-fiber laser pump beam is co-aligned with the MO output. Both beams are focused for optimal mode overlap of around 100 µm radius with 15 cm focal length lenses (L_{MO} and L_{PA}) for the *Z*-cavity or 80 µm with 5 cm focal length lenses for the *L*-cavities.

4. Experimental results

The *Z*- and *L*-cavity oscillators were optimized for highest output (*Z*-cavity) or just below the damage threshold for the AR coatings (*L*-cavities). All experiments were done with the laser samples cooled with circulating water maintained at 10° C. Experimentally, it was determined that the L_b-cavity was easily out-performed by the L_a-cavity, possibly due to additional losses from the intra-cavity lens (~5% per pass). Once an MO was optimized in this way, the PA pump power was then varied to test the system and compare to the theoretical model. The data shown in Fig. 4 represents the best performance of each of the MOPA configurations. From this, it can be seen that the L_a-cavity is better suited for power scaling than the *Z*-cavity. This is likely due to the limited ability of the fixed-angle curved mirrors in the *Z*-cavity to compensate for the increasing astigmatism from the Brewster-angle thermal lens in the gain element. However, it should be noted that the output from the *Z*-cavity is tunable and, due to the poor performance of the L_b-cavity, this is not an option in the linear cavity configuration.

The experimental data follows the model-predicted performance at lower pump powers when thermal lensing in the amplifier crystal is low. As the thermal lens power increases however, the size of the pump and signal beams are affected by the lens and begin to deviate from the values which were used in the model. This, along with any changes in overlap between the two beams, causes the differences between the model and experiment. Experimental evidence also showed that longer amplifier crystals showed little improvement in amplification, supporting the model predictions about pump depletion levels at higher pump powers.

#126243 - $15.00 USD Received 30 Mar 2010; revised 14 Jun 2010; accepted 23 Jun 2010; published 30 Jun 2010

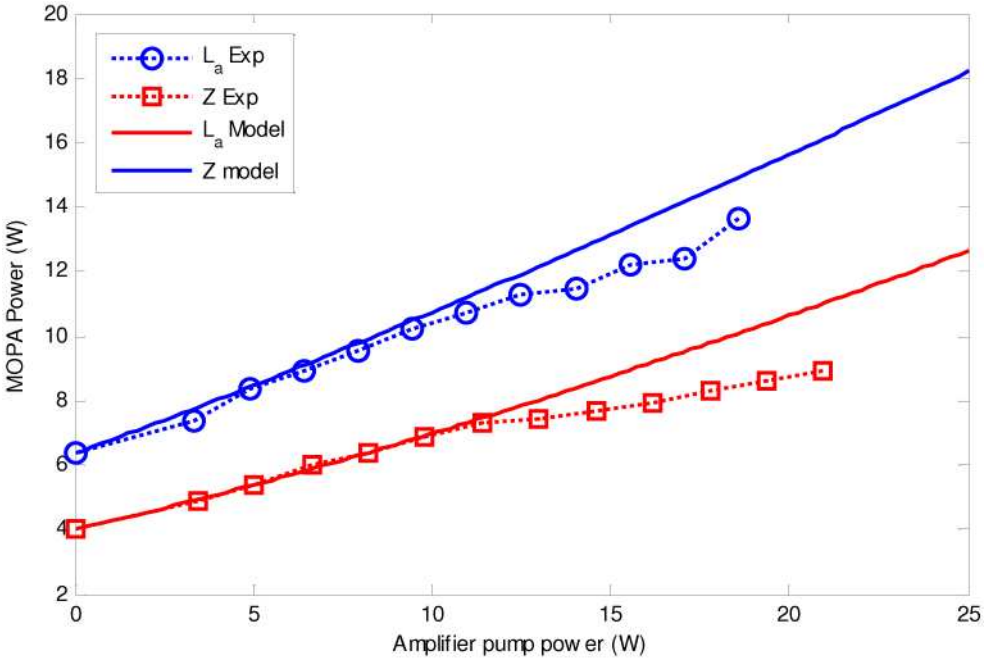

Fig. 4. Power scaling ability of MOPA configurations. Experimental data (discrete points) is compared with model predictions for L_a- and Z-cavities, both with 80 μm and 100 μm spot sizes, respectively.

The output spectrum of the free-running (no grating present) L_b-cavity MO was measured as a function of output power. Spectra were measured by a 2MHz Cal Sensors 256 element PbSe linear detector array coupled to the exit slit of a 750 mm Acton Research Corporation monochromator.. This system was calibrated and optimized using a Yokogawa 735305 optical spectrum analyzer (OSA) and a 150 W IPG Tm fiber laser. The OSA showed a 0.2 nm linewidth for the 150 W IPG laser and after proper positioning of the array at the focal plane and adjustment of the monochromator slit widths, similar resolution was achieved with the spectrometer system. Figure 5 shows that the width of the collection of output peaks of the laser is not a function of pump power, however, the weighted average wavelength increases with pump power, going from 2415 to 2442 nm. There are a number of thermal effects which could be postulated to shift the average output wavelength in either direction, but it is difficult to predict which will dominate. A shift to the longer wavelengths could be due to higher temperatures in the crystal affecting non-radiative transitions for higher energy levels.

#126243 - $15.00 USD Received 30 Mar 2010; revised 14 Jun 2010; accepted 23 Jun 2010; published 30 Jun 2010

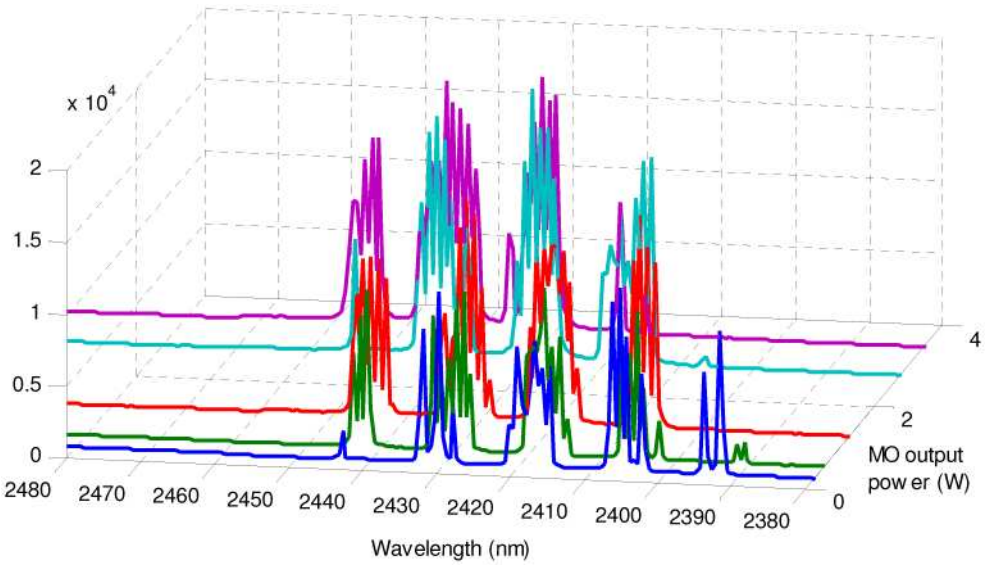

Fig. 5. Output spectrum of free-running L_b-cavity as a function of output power showing a shift to higher wavelengths at increased power.

Representative tunable output characteristics of the amplified, grating equipped *Z*-cavity are shown in Fig. 6. A maximum power of 8.9 W was achieved at 2450 nm with tunable lasing over the 2275-2700 nm range, which was limited by grating efficiency and wavelength-dependent coating reflectivity. Figure 6 shows the dependence of the measured output power on wavelength. The linewidths at all measured points were less than 2 nm.

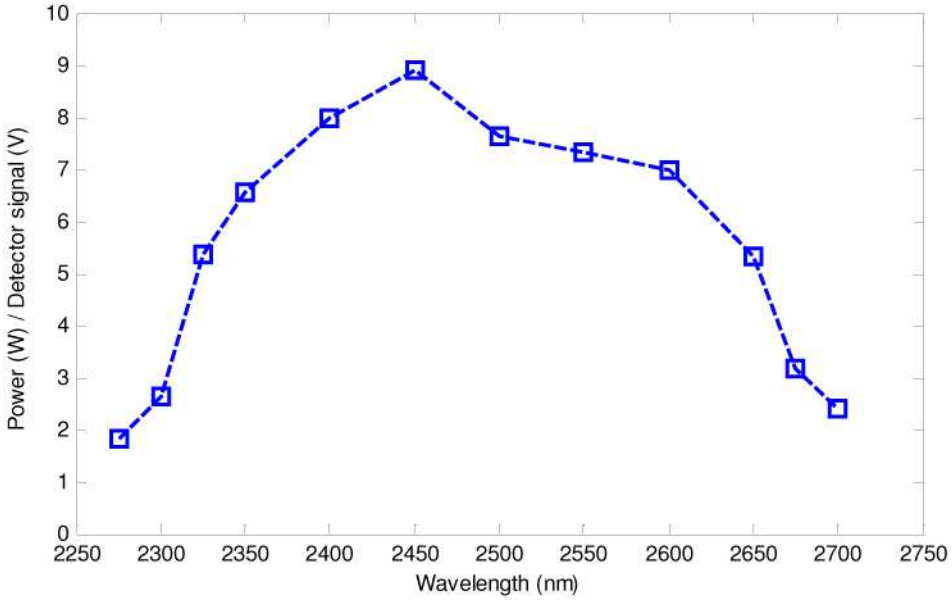

Fig. 6. Tunable output power of *Z*-cavity over 400 nm which was limited by mirror reflectivities and grating efficiency.

One of the goals of the MOPA configuration is an improvement in the beam quality for a given output power. The need for this can be understood by looking at the near-field beam profile of the MO output. Figure 7 shows a single-frame excerpt from a video showing the near-field beam profile of the L_b-cavity as a function of decreasing pump power. The cavity

#126243 - $15.00 USD Received 30 Mar 2010; revised 14 Jun 2010; accepted 23 Jun 2010; published 30 Jun 2010

will run stable in one mode until the power changes enough to allow or cause a shift to a new mode. This type of transition period in the cavity is marked by unstable and fluctuating output powers and beam quality. On the other hand, with a MOPA system, the MO could be placed in a stable region while the system power output is varied by the PA, allowing for more stable overall output power and quality.

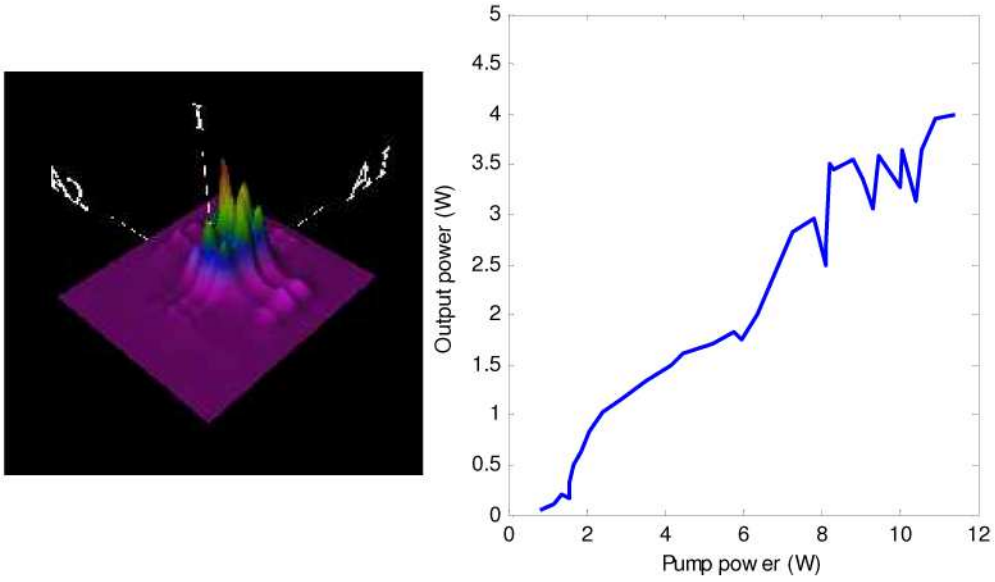

Fig. 7. Single-frame excerpt (left) from video showing near-field beam profile changes of L_b-cavity as a function of decreasing pump power. (Media 1) starts with maximum pump power and ends at zero pump power. Transitions between different modes cause instability in power output (right).

The ability of the MOPA system to achieve higher output powers while maintaining beam quality was tested by measuring the M^2 of the L_a-cavity. At 1 W, the cavity had an M^2 of 1.2 and at 3 W it had an M^2 of 1.8. With the MO running at 1 W and amplified to 3 W with the PA, the system had an M^2 of 1.3. This reinforces the idea that a MOPA system can be used to power scale a system where other issues may limit oscillator operation.

5. Conclusion

In conclusion, we have demonstrated a CW Cr^{2+}:ZnSe MOPA laser with output power of 14 W and amplifier gain of 2X. We developed an amplifier model for co-linearly pumped Cr^{2+}:ZnSe, which compares well with our experimental data. Use of a MOPA configuration allowed us to demonstrate high-power and good beam quality in a Cr^{2+}:ZnSe laser. In addition, we demonstrated single-knob tunability at multi-watt powers over a 400 nm tuning range.

As is common with chromium-doped II-VI lasers, thermal effects limited the output power and beam quality of this setup. Improvements in cooling are needed to take full advantage of the available pump power and increase system stability. This MOPA system will be evaluated with additional MO configurations to study the optimal operating conditions and increase output laser power. Thermal management techniques will continue to be improved in an effort to reduce thermal instability in the oscillator. Improvements will also be made to the model to incorporate thermal lens modeling and effects.

Acknowledgements

The authors would like to thank S. Mirov, V. Fedorov and I. Moskalev (University of Alabama – Birmingham) for extensive discussions on modeling the nature of Cr^{2+} as well as

#126243 - $15.00 USD Received 30 Mar 2010; revised 14 Jun 2010; accepted 23 Jun 2010; published 30 Jun 2010

experimental collaboration. The authors would also like to acknowledge their colleagues and collaborators P. Powers (University of Dayton), T. Wagner, R. Bedford, R. Peterson, J. Evans, C. Phelps, S. Hegde and J. McCurdy (Air Force Research Lab) as well as funding support by the Air Force Office of Scientific Research and the Sensors Directorate of the Air Force Research Laboratory.

#126243 - $15.00 USD Received 30 Mar 2010; revised 14 Jun 2010; accepted 23 Jun 2010; published 30 Jun 2010